The influence of cloud radiative effects on the large-scale atmospheric circulation

Ying Li, * and David W. J. Thompson

Department of Atmospheric Science, Colorado State University, Fort Collins, Colorado, USA

Sandrine Bony

Laboratoire de Météorologie Dynamique, IPSL, CNRS, Université Pierre et Marie Curie, Paris, France

* *Corresponding author address:* Ying Li, Department of Atmospheric Science, Colorado State University, 3915 W. Laporte Ave. Fort Collins, CO 80521

E-mail: yingli@atmos.colostate.edu

ABSTRACT

The influence of clouds on the large-scale atmospheric circulation is examined in numerical simulations from an atmospheric general circulation model run with and without cloud radiative effects.

In the extratropics of both hemispheres, the primary impacts of cloud radiative effects on the circulation include: 1) increases in the meridional temperature gradient and decreases in static stability in the midlatitude upper troposphere; 2) strengthening of the midlatitude jet; 3) increases in extratropical eddy kinetic energy; and 4) increases in precipitation at middle latitudes but decreases at subtropical latitudes. In the tropics, the primary impacts of cloud radiative effects include: 1) eastward wind anomalies in the tropical upper troposphere/lower stratosphere (UTLS); and 2) reductions in tropical precipitation.

The impacts of cloud radiative effects on the atmospheric circulation are interpreted in the context of a series of dynamical and physical processes. The changes in the extratropical circulation and precipitation are consistent with the influence of cloud radiative effects on the baroclinicity and eddy fluxes of momentum in the extratropical upper troposphere; the changes in the zonal wind in the UTLS with the influence of cloud radiative effects on the amplitude of the equatorial planetary waves; and the changes in the tropical precipitation with the energetic constraints on the tropical troposphere.

The results make clear that cloud radiative effects have a pronounced influence on the atmospheric circulation not only at tropical latitudes, but at extratropical latitudes as well. They highlight the critical importance of simulating correctly cloud radiative effects in global climate models.

1. Introduction

Accurate simulations of the atmospheric general circulation are a necessary condition for interpreting climate variability and predicting the climate response to external forcings. However, climate models exhibit a wide range of biases in their simulations of the current climate, and a major source of such biases stems from cloud processes and their role in the general circulation (e.g., Möbis and Stevens 2012; Ceppi et al. 2012; Oueslati and Bellon 2013; Stevens and Bony 2013). One of the ways clouds can affect the atmospheric circulation is through their influence on the radiative heating of the atmosphere.

Cloud radiative effects have long been recognized to influence the Earth's radiation budget. They have been quantified for decades at the top of the atmosphere (TOA; Ramanathan et al. 1989; Harrison et al. 1990; Hartmann et al. 1992; Loeb et al. 2009), and recent advances in remote sensing have make it possible to also quantify them at the surface and *within* the atmosphere (L'Ecuyer et al. 2008; Su et al. 2010; Allan 2011; Kato et al. 2011; Haynes et al. 2013). On global scales, the net cloud radiative effects within the atmosphere (defined as the difference in cloud radiative effects between the surface and TOA) are surprisingly small due to the compensation between cooling due to low clouds at high latitudes and warming due to high clouds in the tropics. But on local and even synoptic scales, cloud radiative effects within the atmosphere can readily reach several tens of W m^{-2}. Since they contribute to atmospheric diabatic heating, cloud radiative effects within the atmosphere can have a profound influence on the large-scale atmospheric circulation.

Early studies using simulations with numerical models reveal that atmospheric cloud radiative effects play a prominent role in determining the mean *tropical* circulation (Slingo and Slingo 1988; Randall et al. 1989; Sherwood et al. 1994; Tian and Ramanathan 2003). Other studies suggest that cloud radiative effects also play a role in tropical intraseasonal variability (Lee et al. 2001; Raymond 2001; Fuchs and Raymond 2002; Bony and Emanuel 2005; Zurovac-Jevtić et al. 2006).

Surprisingly, the influence of cloud radiative effects on the *extratropical* atmospheric

circulation has received comparatively little attention. Ceppi et al. (2012) argue that that model biases in shortwave cloud radiative forcing lead to biases in surface temperatures that induce biases in the latitude of the Southern Hemisphere midlatitude jet; (Ceppi et al. 2014) suggest that trends in shortwave cloud radiative forcing lead to trends in the midlatitude jet. Li et al. (2014a) argue that the TOA cloud radiative effects associated the northern annular mode act to shorten the timescale of its attendant temperature anomalies. Grise et al. (2013) and Grise and Polvani (2014) argue that changes in cloud radiative effects associated with poleward shifts in the midlatitude jet can lead to significant global-mean warming in coupled climate models. But for the most part, the physical mechanisms through which cloud radiative effects influence the large-scale extratropical atmospheric flow remain unclear.

Here we examine the influence of cloud radiative effects on the large-scale atmospheric circulation by exploiting numerical simulations performed under the auspices of the Cloud Feedback Model Intercomparison Project (CFMIP), in which clouds are made transparent to radiation. The simulations, referred to as COOKIE (the Clouds On-Off Klima Intercomparison Experiment, Stevens et al. 2012), allow us to assess the impact that atmospheric cloud radiative effects exert on the atmosphere for a given surface boundary condition. The COOKIE simulations include two primary types of experiments, both of which are run with an atmospheric general circulation model (AGCM) forced with the same observed sea-surface temperatures: 1) control simulations that include the full suite of model cloud radiative effects ("*clouds-on*" experiments); and 2) perturbed simulations in which the model cloud radiative effects are turned off in the radiative computation ("*clouds-off*" experiments). The differences between the *clouds-on* and *clouds-off* experiments reveal the impact of cloud radiative effects on the model climate.

The paper is organized as follows: Section 2 reviews details of the COOKIE simulations and diagnostic techniques. Section 3 examines the long-term mean, zonal-mean circulation in the control (*clouds-on*) experiment. The impacts of cloud radiative effects on the model zonal-mean circulation are documented in Section 4 and interpreted in Section 5. Section 6

summarizes key results.

2. Model and diagnostic details

a. The COOKIE simulations

The COOKIE simulations used in this study are all run using the atmospheric component of the Institute Pierre Simon LaPlace (IPSL) coupled climate model (version IPSL-CM5A-LR; Dufresne et al. 2013). Following the CMIP5 protocol (Taylor et al. 2012), the AGCM is forced by observed monthly-mean SSTs and sea-ice concentration over the 30 year period 1979–2008. The AGCM output is available on a 3.75° latitude × 1.875° longitude mesh and at 39 vertical levels (provided on a hybrid sigma pressure coordinate system). Details of the physics packages used in the IPSL AGCM are provided in Hourdin et al. (2006).

In the majority of the study, we will compare the long-term mean, zonal-mean circulation between two types of experiments: the "*clouds-on*" and "*clouds-off*" simulations (referred to as "amip" and "offamip" experiments, respectively, in Stevens et al. 2012). Select results will draw from additional COOKIE simulations: 1) a 30 year "*boundary layer clouds-off*" simulation (referred to as "offpblamip" in Stevens et al. 2012), in which only planetary boundary layer clouds are made transparent to radiation; and 2) the five year "*aquaplanet clouds-on*" and "*aquaplanet clouds-off*" simulations (referred to as "aquaControl" and "offaquaControl" in Stevens et al. 2012), which are identical to the "*clouds-on*" and "*clouds-off*" experiments, except that they are run in an aquaplanet configuration (see Stevens et al. 2012 for details).

b. Diagnostic details

The following diagnostic tools are used to characterize and interpret the impacts of cloud radiative effects on the atmospheric circulation.

The static stability (N^2) is defined as $\frac{g}{\theta}\frac{\partial \theta}{\partial z}$, where g is 9.81 m s^{-2} and θ is potential tem-

perature, and tropopause height is identified using the World Meteorological Organization lapse rate definition. The zonal-mean eddy kinetic energy (EKE) is defined as $0.5\times[u^{*2}+v^{*2}]$, the zonal-mean eddy fluxes of momentum as $[u^*v^*]$, and the zonal-mean eddy fluxes of heat as $[v^*T^*]$, where brackets denote the zonal-mean and the * denote departures from the zonal-mean. The eddy fluxes are calculated first from daily-mean output and then averaged over all days in the integration.

The Eady growth rate provides a quantitative estimate of the growth rate of baroclinic eddies (Lindzen and Farrell 1980; Hoskins and Valdes 1990) and is defined as:

$$\sigma_D = 0.31g\frac{1}{N}\frac{1}{T}\left|\frac{\partial T}{\partial y}\right|, \tag{1}$$

where N is the Brunt-Väisälä frequency, a measure of static stability, and $\left|\frac{\partial T}{\partial y}\right|$ meridional temperature gradient. The Eady growth rate measures the baroclinicity of the flow and thus the potential energy available for the growth of extratropical storms. The relative contribution of $\left|\frac{\partial T}{\partial y}\right|$ to the total changes in the Eady growth rate between the *clouds-on* and *clouds-off* simulations was found by setting N to its *clouds-on* value in the calculation; the relative contribution of N by setting $\left|\frac{\partial T}{\partial y}\right|$ to its *clouds-on* value.

3. The long-term mean atmospheric circulation and cloud radiative effects in the "*clouds-on*" experiment

a. The atmospheric circulation in the clouds-on experiment

Figure. 1 reviews the zonal-mean circulation of the IPSL model in the control "*clouds-on*" experiment. The results are averaged over all 30 years of the integration. They are shown to provide context for the effects of the cloud radiative effects on the model circulation, as discussed in the following section.

The predominant features in the long-term mean control (*clouds-on*) circulation include:

- Large meridional temperature gradients and pronounced westerlies in the subtropical upper troposphere (contours in panels a and b).

- Surface westerlies at midlatitudes and easterlies in the tropics (contours in panel a) consistent with the eddy fluxes of momentum in the upper troposphere (shading in panel a).

- Maxima in the eddy fluxes of heat near the surface at $\sim 50^\circ$ latitude and near 250 hPa at $\sim 40^\circ$ latitude (shading in panel b).

- Large maxima in zonal-mean eddy kinetic energy centered near 250 hPa between 30°–60° latitude (panel c). The maxima in eddy kinetic energy lie immediately above the maxima in the region of largest baroclinic wave growth (i.e., the Eady growth rate; panel d).

- A minimum in zonal-mean static stability in the tropical upper troposphere and paired maxima in the extratropical lower stratosphere (panel e; the extratropical maxima are consistent with the tropopause inversion layer, Birner 2006).

- A maximum in cloud fraction in the upper tropical troposphere consistent with deep convection; minima in cloud fraction in the subtropics consistent with the descending branch of the Hadley Cell; maxima in cloud fraction in the midlatitude troposphere consistent with extratropical cyclones; and a maximum in low-level clouds over the Southern Ocean. Note that the zonal-mean distribution of clouds in the IPSL model is broadly consistent with the distribution of cloud amounts derived from CloudSat/CALIPSO observations (Haynes et al. 2007; Mace et al. 2007, 2009).

b. Atmospheric cloud radiative effects in the clouds-on experiment

Figure 2 shows the attendant latitude/height structure of the long-term mean, zonal-mean cloud-induced radiative heating rates in the *clouds-on* experiment. Panel a) shows

the longwave component; panel b) the shortwave component; and panel c) the total heating rates. At all levels, the cloud-induced radiative heating rates are defined as the difference between the all-sky and clear-sky radiative heating rates, and thus represent the perturbation radiative heating rates induced by the model clouds. Note that it is the inclusion of this cloud forcing in Fig. 2 that drives the differences in the atmospheric circulation between the two types of experiments.

The cloud-induced longwave radiative heating rates are about 3–4 times larger than the shortwave heating rates. The relatively small amplitudes of the shortwave heating rates within the atmosphere are due to the offsetting effects of clouds on shortwave radiation at the TOA and surface. For example: An increase in clouds leads to a reduction in shortwave heating not only at the TOA, but also at the surface, thus leading to relatively small net shortwave heating within the atmosphere. The much larger role of longwave cloud radiative effects at atmospheric levels is consistent with results shown in observational studies (Kato et al. 2008; Allan 2011; Haynes et al. 2013).

The cloud-induced total radiative heating rates (panel c) have a distinct latitude/height structure. The radiative effects of clouds in the IPSL model are positive in the middle troposphere but negative in the upper troposphere near the tropopause level. The regions of positive cloud radiative effects are consistent with the trapping of outgoing longwave radiation from the middle troposphere by clouds in the upper troposphere; the regions of negative cloud radiative effects are consistent with the increased emission of longwave radiation by clouds in the upper troposphere. The heating of the middle troposphere is larger in the tropics than it is in the polar regions, likely due to the larger optical depth of clouds in the tropics (Kato et al. 2008).

In the lower troposphere, the net radiative effect of clouds is negative in the boundary-layer atmosphere but positive near the surface (the heating near the surface is not shown in the figure). At middle and high latitudes, the negative radiative forcing in the boundary layer is larger than the positive radiative forcing in the middle troposphere. Hence, as

noted in observations in Kato et al. (2008), Allan (2011), and Haynes et al. (2013), the vertically integrated cloud radiative effect within the atmosphere is negative at middle and high latitudes.

4. The influence of cloud radiative effects on the large-scale atmospheric circulation

In this section we document the response of the zonal-mean atmospheric circulation to the atmospheric cloud radiative effects shown in Fig. 2c. To do so, we examine the differences in the long-term mean, zonal mean atmospheric circulation in the IPSL model between the 30-year *clouds-on* and *clouds-off* experiments. The mechanisms of the response are explored in Section 5.

Figures 3–6 explore the impacts of the cloud radiative effects on the zonal-mean, long-term mean atmospheric circulation. As noted above, the effects of the cloud radiative effects are given by the differences between the long-term means in the *clouds-on* and *clouds-off* experiments. The statistical significance of the differences is assessed using a two-tailed test of the t-statistic for the difference of means, where we assume there are 2 degrees of freedom in each calendar year.

Figure 3 examines the influences of the cloud radiative effects on the zonal-mean temperature, wind and eddy-kinetic energy fields. In all fields, the response to cloud radiative effects exhibits a high degree of hemispheric symmetry. The primary features include:

- Cooling in the extratropical lower stratosphere/upper troposphere that peaks near ∼200 hPa and 55° latitude, juxtaposed against warming in the free troposphere that peaks near ∼200 hPa at the Equator (Fig. 3a). The warming exceeds 2K throughout the tropical troposphere and is consistent with the positive cloud radiative effects in the middle and upper troposphere (Fig. 2c). The cooling exceeds 5K throughout much of

the extratropical lower stratosphere and lies above the negative cloud radiative effects near the tropopause (Fig. 2c). Since the cooling of the extratropical tropopause region is not clearly collocated with the negative cloud radiative effects (as shown in Fig. 2c), it must be driven dynamically, as indicated further below.

- Lifting of the tropopause at all latitudes (the heights of the tropopause in the *clouds-on* and *clouds-off* experiments are indicated by the solid and dashed lines, respectively). The lifting of the tropopause is consistent with the modified thermal structure of the atmosphere (Fig. 3a).

- Eastward wind anomalies in the extratropical zonal flow between ∼30°–45° latitude juxtaposed against weak (but significant) westward anomalies poleward of ∼60° (Fig. 3b). The vertical shear of the wind anomalies at upper levels is mandated by the large meridional gradients in temperature at the tropopause level (Fig. 3a). The surface component of the wind anomalies is consistent with the attendant changes in the eddy fluxes of momentum, as discussed below.

- Eastward wind anomalies centered about the Equator in the tropical upper troposphere/lower stratosphere region (UTLS; Fig. 3b). Immediately poleward of the Equator, the wind anomalies are consistent with the vertical shear of the flow required by the anomalous meridional temperature gradients in the subtropical UTLS. But at the Equator, the wind anomalies must be driven by momentum fluxes due to either the mean meridional circulation or eddies (e.g., Dima et al. 2005; Kraucunas and Hartmann 2005; Dima and Wallace 2007). The response of the eastward wind anomalies in the tropical UTLS region will be discussed later in Section 5b.

- Widespread increases in eddy kinetic energy (EKE) centered in both the extratropical and tropical UTLS (Fig. 3c). The changes in extratropical EKE account for a ∼30% increase in eddy amplitudes (compare Fig. 3c and Fig. 1c). They project strongly onto the leading pattern of storm track variability documented in Lau (1988) and Wettstein

and Wallace (2010), and also onto the positive polarity of the baroclinic annular mode (Thompson and Woodworth 2014; Thompson and Li 2014).

Figure 4 shows the attendant changes in the fields of the eddy fluxes of momentum (contours in left panel) and heat (contours in right panel). The changes in the eddy fluxes are superposed on the changes in the zonal-mean zonal wind (shading in left panel) and temperature (shading in right panel) reproduced from Fig. 3. The primary responses in the eddy fluxes again exhibit a high degree of hemispheric symmetry, and include:

- Anomalously poleward momentum fluxes centered ∼40° juxtaposed against anomalously equatorward momentum fluxes centered ∼60° (note that poleward fluxes are denoted by positive values in the Northern Hemisphere but negative values in the Southern Hemisphere). The associated convergence of the eddy flux of eastward momentum between ∼40°–60° must drive the anomalous surface eastward flow there; the divergence of the eddy flux of eastward momentum poleward of ∼60° must drive the anomalous surface westward flow there. The weak eddy momentum fluxes in the tropical UTLS imply convergence of eastward momentum at the Equator.

- Anomalously poleward heat fluxes in the upper troposphere and lower stratosphere between ∼20°–50° collocated with anomalously equatorward heat fluxes centered ∼250 hPa at subpolar latitudes. (The anomalous eddy fluxes of heat are not shown below 500 hPa where they are noisy, amorphous, and uniformly insignificant). The anomalous eddy fluxes of heat are oriented down the gradient of the temperature anomalies and thus can be interpreted as responding to (as opposed to driving) the changes in atmospheric temperature.

Figure 5 shows the associated changes in static stability (left) and cloud fraction (right). As also indicated by the changes in temperature (Fig. 3a), the cloud radiative effects leads to widespread decreases in atmospheric static stability near the tropopause and relatively weak increases in static stability in the extratropical lower stratosphere (the associated changes

in tropopause height are reproduced from Fig. 3a). The cloud radiative effects also lead to increases in cloud fraction that peak in the extratropical upper troposphere (Fig. 5b). The increases in extratropical cloud fraction project strongly onto the decreases in atmospheric static stability, consistent with the linkages between free tropospheric cloud incidence and static stability found in observations (Li et al. 2014b).

Finally, Figure 6 compares the long-term mean, zonal-mean precipitation in the *clouds-on* and *clouds-off* experiments. In both experiments, the long-term mean precipitation exhibits a maximum in the deep tropics that peaks north of the equator, minima at subtropical latitudes, and maxima in the extratropical stormtrack regions, which is broadly consistent with the long-term mean precipitation found in other climate models (Dai 2006; Lin 2007). Cloud radiative effects lead to increases in precipitation at mid-high latitudes (indicated by the red shading between 40°–60°) and decreases at subtropical latitudes (indicated by the blue shading between 20°–40°). They also lead to decreases in precipitation at tropical latitudes between 20°S–20°N. Interestingly, similar experiments focusing on the impact of boundary-layer cloud radiative effects show that low-cloud radiative effects tend to increase tropical precipitation (Fermepin and Bony 2014). Therefore the results shown here imply that the influence on tropical precipitation of free-tropospheric clouds (which radiatively heat the atmosphere) dominates that of planetary boundary layer clouds (which radiatively cool the atmosphere).

5. Interpretation

The response of the zonal-mean atmospheric circulation to cloud radiative effects is consistent with a series of dynamical and thermodynamical processes. As discussed below, the response of the extratropical atmospheric circulation is consistent with the influence of cloud radiative effects on upper tropospheric baroclinicity and the amplitude of baroclinic waves. In the tropics, it is consistent with the influence of cloud radiative effects on the amplitude

of the equatorial Rossby waves, and the energy balance requirements in the free tropical troposphere. We begin with a discussion of the extratropical response.

a. Extratropical circulation

The eddy fluxes of momentum and heat play a central role in the extratropical circulation. Both are linked to the amplitudes of midlatitude baroclinic waves: anomalously large amplitude of midlatitude eddies derive from anomalously large poleward fluxes of heat (Holton 2004; Vallis 2006). They can also lead to anomalously large wave fluxes of momentum through the lifecycle of baroclinic waves (Simmons and Hoskins 1978; Edmon et al. 1980). The amplitudes of midlatitude eddies, in turn, are closely connected to the amplitude of the extratropical baroclinicity, which provides the fundamental source of energy for developing baroclinic waves. As noted in Section 2, the growth rate of developing baroclinic waves can be estimated from the Eady growth rate.

The response of the extratropical atmospheric circulation to cloud radiative effects is qualitatively consistent with the changes in baroclinicity and thus wave growth in the extratropical upper troposphere. Figure 7 shows the changes in the extratropical Eady growth rate between the *clouds-on* and *clouds-off* experiments. In the extratropical upper troposphere, the amplitude of the Eady growth rate is $\sim$30% larger in the *clouds-on* experiment than it is in the *clouds-off* experiment. The response peaks near 300 hPa and at $\sim$40°, and is closely collocated with the long-term mean maxima in the Eady growth rate in the *clouds-on* experiment (see Fig. 1d). The increases in the Eady growth rate derive from both increases in the meridional temperature gradient (Fig. 7b; the numerator in equation (1)) and decreases in the static stability (Fig. 7c; the denominator in equation (1)) in the extratropical upper troposphere.

The increases in the Eady growth rate in the extratropical upper troposphere correspond to a destabilization of the extratropical upper troposphere to baroclinic wave growth. The destabilization of the flow is consistent with the increases in the poleward eddy fluxes of

heat (Fig. 4b) and eddy kinetic energy (Fig. 3c) at middle latitudes: i.e., regions where the flow is more baroclinically unstable are marked by both anomalously poleward fluxes of heat by atmospheric eddies and enhanced eddy amplitudes. The much larger eddy amplitudes are also consistent with enhanced "stirring" of the midlatitude circulation by baroclinic instability. Stirring of the extratropical circulation leads to the generation of Rossby waves in the upper troposphere waves that propagate meridionally away from - and flux eastward momentum into - the stirring region (Held 2000; Vallis 2006). Hence, the changes in the eddy fluxes of momentum indicated in Fig. 4a are at least qualitatively consistent with the influence of cloud radiative effects on the amplitude of baroclinic waves in the extratropical middle and upper troposphere.

The changes in the eddy fluxes of momentum indicated in Fig. 4a, in turn, play a central role in the changes in vertical motion at extratropical latitudes (indicated in Fig. 8). At extratropical latitudes, the zonal-mean (Eulerian) meridional overturning circulation is driven primarily by the eddy fluxes of momentum (Vallis 2006; the fluxes of momentum by the mean meridional flow contribute primarily at low latitudes). For example, eastward forcing due to the convergence of the eddy flux of eastward momentum is balanced by westward forcing due to the Coriolis torque acting on the meridional flow, and vice versa. In the case of the response to cloud radiative effects, the anomalous convergence of the eddy flux of eastward momentum in the upper troposphere between $\sim$40°–60° latitude (Fig. 4a) must be balanced in part by the Coriolis torque acting on anomalously equatorward flow. As indicated in Fig. 8, both hemispheres are, in fact, marked by equatorward flow at middle latitudes, consistent with the force balance requirements noted above. Similar reasoning applies to the anomalous divergence of the eddy flux of eastward momentum and poleward flow at subpolar latitudes.

The changes in the meridional motion induced by the eddy fluxes of momentum play an important role in the changes in extratropical precipitation. From continuity of mass, the anomalous meridional flow driven by the momentum fluxes must be accompanied by rising

motion centered ∼50° and descending motion centered ∼30° (Fig. 8). Comparing Figs. 6 and 8, it is clear that regions with anomalous ascending motion at mid-high latitudes are closely collocated with regions of increased precipitation, whereas regions with anomalous descending motion at subtropical latitudes are closely collocated with regions of decreased precipitation. Hence, the changes in extratropical precipitation induced by the cloud radiative effects can be viewed as fundamentally driven by the anomalous eddy momentum fluxes aloft which, in turn, are driven by the influence of the cloud radiative effects on the extratropical upper tropospheric baroclinicity.

b. Tropical circulation

In the tropics, the primary influence of cloud radiative effects on the zonal-mean atmospheric circulation include: 1) eastward wind anomalies in the UTLS and 2) a reduction in precipitation. The former can be traced to increased amplitude of the equatorial planetary waves; the latter to the energetic constraints on large-scale tropical precipitation.

The equatorial waves are driven by zonally asymmetric heating in the tropical atmosphere. The prominent latent heating over the western tropical Pacific induces an off-equatorial Rossby wave response to the west of heating, and a Kelvin wave response to the east (e.g., Gill 1980; Highwood and Hoskins 1998; Dima et al. 2005; Dima and Wallace 2007). The equatorial Rossby waves propagate out of the deep tropics and hence flux eastward momentum into the tropical UTLS (Dima et al. 2005; Dima and Wallace 2007).

Figure 9 indicates the horizontal structure of the long-term mean 150-hPa geopotential height in the *clouds-on* (top) and *clouds-off* (bottom) experiments. The results show the wave component of the 150 hPa geopotential height field, i.e., the geopotential height field minus its zonal mean. Cloud radiative effects evidently play a key role in governing the structure of the geopotential height field at 150 hPa. In the *clouds-on* experiment, the 150-hPa geopotential height field is characterized by paired off-equatorial ridges centered ∼120°–160°E and troughs centered ∼110–150°W. The structure of the tropical 150 hPa

geopotential height field in the *clouds-on* experiment is qualitatively similar to that in the observations (Dima et al. 2005; Dima and Wallace 2007; compare with Grise and Thompson 2012 Fig. 1b). In the *clouds-off* experiment, the amplitudes of the off-equatorial ridges and troughs are notably weaker than they are in the *clouds-on* experiment. The results in Fig. 9 imply that observed Equatorial waves are affected not only by latent heating but also the associated cloud-induced radiative heatings. The more pronounced structure of the equatorial planetary waves is consistent with the increases in tropical eddy kinetic energy (Fig. 3c), the anomalous equatorward flux of eastward momentum (Fig. 4a), and the anomalous eastward wind anomalies (Fig. 3b) in the tropical upper UTLS found in association with the cloud radiative effects.

The signature of cloud radiative effects on tropical precipitation is not clearly attributable to changes in zonal-mean vertical motion (not shown; the changes in tropical vertical motion are noisy and not significant). Rather they are consistent with the energetic constraints on tropical precipitation (see review by O'Gorman et al. 2012, and reference therein). On large spatial scales, the changes in precipitation are constrained by changes in 1) the radiative cooling of the atmosphere and 2) the surface sensible heat flux. Averaged over the tropics (30°S–30°N), the changes in the vertically integrated radiative heating between the *clouds-on* and *clouds-off* experiments is +13.3 W m^{-2}, which is the sum of the changes in the clear-sky radiative cooling ($\Delta R_{clear} = -4.6$ W m^{-2}) and atmospheric cloud radiative effect ($\Delta ACRE = 17.9$ W m^{-2}). The heating by the radiative effects of clouds in the *clouds-on* experiment is balanced by reductions (relative to the *clouds-off* experiment) in: 1) the latent heating of condensation ($L\Delta P = -8.9$ W m^{-2}) and 2) the upward surface sensible heat flux ($\Delta SH = -3.7$ W m^{-2}). Hence the heating of the tropical atmosphere by cloud radiative effects (Fig. 2c) is primarily balanced by a reduction in the latent heating, consistent with the reduction in tropical precipitation evident in the *clouds-on* simulation (Fig. 6).

6. Summary and Discussion

As summarized in Fig. 10, cloud radiative effects impact the atmospheric circulation in several ways:

1) *An increase in baroclinicity and eddy activity in the extratropical upper troposphere.* As discussed in Section 5, the increases in baroclinicity are physically consistent with increases in the kinetic energy, poleward fluxes of heat, and eastward momentum forcing associated with eddies in the midlatitude upper troposphere. The changes in eddy momentum forcing, in turn, drive a dipole in the zonal-mean zonal wind anomalies, with anomalous eastward flow centered $\sim$45° and anomalous westward flow at subtropical latitudes. They also drive changes in vertical motion that subsequently lead to increases in precipitation at mid-high latitudes (40°–60°) and decreases in the subtropics (20°–40°).

2) *Eastward flow in the tropical UTLS region.* The eastward flow is consistent with the influence of the zonally asymmetric structure of the tropical atmospheric cloud radiative effects on the amplitude of the equatorial planetary waves.

3) *Decreases in tropical precipitation.* The decreases in tropical precipitation are consistent with a reduction in tropical tropospheric latent heating, which is required to balance the increases in radiative heating due to cloud radiative effects there.

We have focused on the atmospheric response to cloud radiative effects imposed at all levels and latitudes. We tested whether the primary changes found in this study are due to clouds in the planetary boundary layer by examining atmospheric circulation response in COOKIE experiments in which only the radiative effects of boundary layer clouds are turned off (see Section 2a). Preliminary results (not shown) indicate that the notable changes in tropospheric eddy activity shown here are not simulated in those experiments. Hence the effects on the atmospheric circulation of planetary boundary layer clouds is seemingly smaller than the effects on the circulation of free tropospheric clouds. We also tested the results in

the aqua-planet configuration of the IPSL model, and found changes in tropospheric eddy activity similar to those documented here (not shown). Hence, the unique land-sea geometry of a particular hemisphere does not play a key role in the zonal-mean response indicated here.

The findings shown here highlight the key role of cloud radiative effects in determining the structure of the large-scale atmospheric circulation. The results are derived from a single climate model (the IPSL model), but since the responses follow from a series of physically consistent relationships, we expect they will prove robust in any climate model with cloud radiative effects similar to those indicated in Fig 2. The results make clear that model biases in tropospheric cloud radiative effects will lead to substantial biases in simulations of the atmospheric flow not only at tropical latitudes, but at extratropical latitudes as well (see also Ceppi et al. 2012; Grise et al. 2013).

The findings raise several obvious questions for future work. For examples: What is the relative role of tropical and extratropical cloud radiative effects in driving the extratropical atmospheric response indicated here? Is the atmospheric response to cloud radiative effects robust in other climate models? How does the atmospheric response vary as a function of the seasonal cycle? What is the zonally varying structure of the atmospheric response? And to what extent do changes in the cloud radiative effects impact the time scales and structures of large-scale patterns of atmospheric variability? We are exploring these questions in our ongoing analyses.

Acknowledgments.

We thank Abderrahmane Idelkadi (LMD) for running the "clouds-off" simulation. YL is funded by CloudSAT via NASA JPL and the NSF Climate Dynamics program. DWJT is funded by the NSF Climate Dynamics program.

REFERENCES

Allan, R. P., 2011: Combining satellite data and models to estimate cloud radiative effect at the surface and in the atmosphere, Meteorological Applications. *Meteor. Appl.*, **18**, 324–333.

Birner, T., 2006: Fine-scale structure of the extratropical tropopause region. *J. Geophys. Res.*, **111**, D04 104, doi:10.1029/2005JD006301.

Bony, S. and K. A. Emanuel, 2005: On the role of moist processes in tropical intraseasonal variability: Cloud-radiation and moisture-convection feedbacks. *J. Atmos. Sci.*, **62**, 2770–2789.

Ceppi, P., Y.-T. Hwang, D. M. W. Frierson, and D. L. Hartmann, 2012: Southern Hemisphere jet latitude biases in CMIP5 models linked to shortwave cloud forcing. *Geophys. Res. Lett.*, **39**, L19 708, doi:10.1029/2012GL053115.

Ceppi, P., M. D. Zelinka, and D. L. Hartmann, 2014: The response of the Southern Hemispheric eddy-driven jet to future changes in shortwave radiation in CMIP5. *Geophys. Res. Lett.*, **41**, 3244–3250, doi:10.1002/2014GL060043.

Dai, A., 2006: Precipitation characteristics in eighteen coupled climate models. *J. Climate*, **19**, 4605–4630, doi:10.1175/JCLI3884.1.

Dima, I. and J. M. Wallace, 2007: Structure of the annual-mean equatorial planetary waves in the ERA-40 reanalyses. *J. Atmos. Sci.*, **64**, 2862–2880, doi:10.1175/JAS3985.1.

Dima, I. M., J. M. Wallace, and I. P. Kraucunas, 2005: Tropical angular momentum balance in the NCEP Reanalyses. *J. Atmos. Sci.*, **62**, 282 499–2513.

453 Dufresne, J.-L., et al., 2013: Climate change projections using the IPSL-CM5 earth
454 system model: From CMIP3 to CMIP5. *Climate Dyn.*, **40**, 2123–2165, doi:10.1007/
455 s00382-012-1636-1.

456 Edmon, H. J., B. J. Hoskins, and M. E. McIntyre, 1980: Eliassen-Palm cross sections for the
457 troposphere. *J. Atmos. Sci.*, **37**, 2600–2616.

458 Fermepin, S. and S. Bony, 2014: Influence of low-cloud radiative effects on tropical circulation
459 and precipitation. *J. Adv. Model. Earth Syst*, **06**, doi:10.1002/2013MS000288.

460 Fuchs, V. Z. and D. J. Raymond, 2002: Large-scale modes of a nonrotating atmosphere with
461 water vapor and cloud-radiation feedbacks. *J. Atmos. Sci.*, **59**, 1669–1679.

462 Gill, A. E., 1980: Some simple solutions for heat-induced tropical circulation. *Quart. J. Roy.*
463 *Meteor. Soc.*, **106**, 447–462.

464 Grise, K. M. and L. M. Polvani, 2014: Southern Hemisphere clouddynamics biases in CMIP5
465 models and their implications for climate projections. *J. Climate*, **27**, 6074–6092, doi:
466 10.1175/JCLI-D-14-00113.1.

467 Grise, K. M., L. M. Polvani, G. Tselioudis, Y. Wu, and M. D. Zelinka, 2013: The ozone
468 hole indirect effect: Cloud-radiative anomalies accompanying the poleward shift of the
469 eddy-driven jet in the Southern Hemisphere. *Geophys. Res. Lett.*, **40**, 3688–3692, doi:
470 10.1002/grl.50675.

471 Grise, K. M. and D. W. J. Thompson, 2012: Equatorial planetary waves and their signature
472 in atmospheric variability. *J. Atmos. Sci.*, **69**, 857–874.

473 Harrison, E. F., P. Minnis, B. R. Barkstrom, V. Ramanathan, R. D. Cess, and G. G. Gibso,
474 1990: Seasonal variation of cloud radiative forcing derived from the Earth Radiation
475 Budget Experiment. *J. Geophys. Res.*, **95**, 18 687–18 703.

476 Hartmann, D. L., M. Ockert-Bell, and M. L. Michelsen, 1992: The effect of cloud type on
477 earth's energy balance: Global analysis. *J. Climate*, **5**, 1281–1304.

478 Haynes, J. M., T. H. V. Haar, T. L'Ecuyer, and D. Henderson, 2013: Radiative heating char-
479 acteristics of Earths cloudy atmosphere from vertically resolved active sensors. *Geophys.*
480 *Res. Lett.*, **40**, 624–630, doi:10.1002/grl.50145.

481 Haynes, J. M., Z. Luo, G. L. Stephens, R. T. Marchand, and A. Bodas-Salcedo, 2007: A
482 multipurpose radar simulation package: QuickBeam. *Bull. Amer. Meteor. Soc.*, **88**, 1723–
483 1727, doi:10.1175/BAMS-88-11-1723.

484 Held, I. M., 2000: The General Circulation of the Atmosphere. Proc. Woods Hole
485 Summer School on GFD, 66 pp. Available online at `http://www.gfdl.noaa.gov/`
486 `cms-filesystem-action/user_files/ih/lectures/woods_hole.pdf`.

487 Highwood, E. J. and B. J. Hoskins, 1998: The tropical tropopause. *Quart. J. Roy. Meteor.*
488 *Soc.*, **124**, 1579–1604.

489 Holton, J. R., 2004: *An Introduction to Dynamic Meteorology*. 4th ed., Academic Press, 535
490 pp.

491 Hoskins, B. J. and P. J. Valdes, 1990: On the existence of storm-tracks. *J. Atmos. Sci.*, **47**,
492 1854–1864.

493 Hourdin, F., et al., 2006: The LMDZ4 general circulation model: Climate performance and
494 sensitivity to parametrized physics with emphasis on tropical convection. *Climate Dyn.*,
495 **27**, 787–813, doi:10.1007/s00382-006-0158-0.

496 Kato, S., F. G. Rose, D. A. Rutan, and T. P. Charlock, 2008: Cloud effects on meridional
497 atmospheric energy budget estimated from Clouds and the Earths Radiant Energy System
498 (CERES) data. *J. Climate*, **21**, 4223–4241.

Kato, S., et al., 2011: Improvements of top-of-atmosphere and surface irradiance computations with CALIPSO-, CloudS at-, and MODIS-derived cloud and aerosol properties. *J. Geophys. Res.*, **116**, D19 209, doi:10.1029/2011JD016050.

Kraucunas, I. P. and D. L. Hartmann, 2005: Equatorial superrotation and the factors controlling the zonal-mean zonal winds in the tropic. *J. Atmos. Sci.*, **62**, 371–389.

Lau, N.-C., 1988: Variability of the observed midlatitude storm tracks in relation to low-frequency changes in the circulation pattern. *J. Atmos. Sci.*, **45**, 2718–2743.

L'Ecuyer, T. S., N. B. Wood, T. Haladay, G. L. Stephens, and P. W. Stackhouse, 2008: Impact of clouds on atmospheric heating based on the R04 CloudSat fluxes and heating rates data set. *J. Geophys. Res.*, **113**, D00A15, doi:10.1029/2008JD00995.

Lee, M.-I., I.-S. Kang, J.-K. Kim, and B. E. Mapes, 2001: Influence of cloud-radiation interaction on simulating tropical intraseasonal oscillation with an atmospheric general circulation model. *J. Geophys. Res.*, **106**, 14 219–14 233.

Li, Y., D. W. J. Thompson, Y. Huang, and M. Zhang, 2014a: Observed linkages between the Northern Annular Mode/North Atlantic Oscillation, cloud incidence, and cloud radiative forcing. *Geophys. Res. Lett.*, **41**, 1681–1688, doi:10.1002/2013GL059113.

Li, Y., D. W. J. Thompson, G. L. Stephens, and S. Bony, 2014b: A global survey of the linkages between cloud vertical structure and large-scale climate. *J. Geophys. Res.*, **119**, 3770–3792, doi:10.1002/2013JD020669.

Lin, J.-L., 2007: The double-ITCZ problem in IPCC AR4 coupled GCMs: Ocean-atmosphere feedback analysi. *J. Climate*, **20**, 4497–4525, doi:10.1175/JCLI4272.1.

Lindzen, R. S. and B. Farrell, 1980: A simple approximate result for the maximum growth rate of baroclinic instabilities. *J. Atmos. Sci.*, **37**, 1648–1654.

522 Loeb, N. G., B. A. Wielicki, D. R. Doelling, G. L. Smith, D. F. Keyes, S. Kato, N. Manlo-
523 Smith, and T. Wong, 2009: Toward optimal closure of the Earths top-of-atmosphere
524 radiation budget. *J. Climate*, **22**, 748–766.

525 Mace, G. G., R. Marchand, Q. Zhang, and G. Stephens, 2007: Global hydrometeor occur-
526 rence as observed by CloudSat: Initial observations from summer 2006. *Geophys. Res.*
527 *Lett.*, **34**, L09 808, doi:10.1029/2006GL029017.

528 Mace, G. G., Q. Zhang, M. Vaughn, R. Marchand, G. Stephens, C. Trepte, and D. Winker,
529 2009: A description of hydrometeor layer occurrence statistics derived from the first year
530 of merged CloudSat and CALIPSO data. *J. Geophys. Res.*, **114**, D00A26, doi:10.1029/
531 2007JD009755.

532 Möbis, B. and B. Stevens, 2012: Factors controlling the position of the Intertropical
533 Convergence Zone on an aquaplanet. *J. Adv. Model. Earth Syst*, **4**, M00A04, doi:
534 10.1007/s00382-010-0958-0.

535 O'Gorman, P. A., Allan, R. P. Byrne, and M. P. Previdi, 2012: Energetic constraints on
536 precipitation under climate change. *Surveys in Geophysics*, **33**, 585–608.

537 Oueslati, B. and G. Bellon, 2013: Convective entrainment and large-scale organization of
538 tropical precipitation: Sensitivity of the CNRM-CM5 hierarchy of models. *J. Climate*, **26**,
539 2931–2946, doi:10.1175/JCLI-D-12-00314.1.

540 Ramanathan, V., R. D. Cess, E. F. Harrison, P. Minnis, B. R. Barkstrom, E. Ahmad,
541 and D. Hartmann, 1989: Cloud-radiative forcing and climate: Results from the Earth
542 Radiation Budget Experiment. *Science*, **243**, 57–63.

543 Randall, D. A., Harshvardhan, D. A., Dazlich, and T. G. Corsett, 1989: Interactions among
544 radiation, convection, and large-scale dynamics in a general circulation model. *J. Atmos.*
545 *Sci.*, **46**, 1943–1970.

Raymond, D. J., 2001: A new model of the Madden-Julian Oscillation. *J. Atmos. Sci.*, **58**, 2807–2819.

Sherwood, S. C., V. Ramanathan, T. P. Barnett, M. K. Tyree, and E. Roeckner, 1994: Response of an atmospheric general circulation model to radiative forcing of tropical clouds. *J. Geophys. Res.*, **99**, 20 829–20 845.

Simmons, A. J. and B. J. Hoskins, 1978: The life cycles of some nonlinear baroclinic waves. *J. Atmos. Sci.*, **35**, 414–432.

Slingo, A. and J. M. Slingo, 1988: The response of a general circulation model to cloud longwave radiative forcing. I: Introduction and initial experiments. *Quart. J. Roy. Meteor. Soc.*, **114**, 1027–1062.

Stephens, G. L., 2005: feedbacks in the climate system: A critical review. *J. Climate*, **18**, 237–273.

Stevens, B. and S. Bony, 2013: What are climate models missing? *Science*, **340**, 1053–1054.

Stevens, B., S. Bony, and M. Webb, 2012: Clouds on-off klimate intercomparison experiment (COOKIE). Tech. rep. [Available online at http://www.euclipse.eu/downloads/Cookie.pdf.].

Su, W., A. Bodas-Salcedo, K.-M. Xu, and T. P. Charlock, 2010: Comparison of the tropical radiative flux and cloud radiative effect profiles in a climate model with clouds and the earth's radiant energy system (CERES) data. *J. Geophys. Res.*, **115**, D01 105, doi:10.1029/2009JD012490.

Taylor, K. E., R. J. Stouffer, and G. a. Meehl, 2012: An overview of CMIP5 and the experiment design. *Bull. Amer. Meteor. Soc.*, **93**, 485–498, doi:10.1175/BAMS-D-11-00094.1.

Thompson, D. W. J. and Y. Li, 2014: Baroclinic and barotropic annular variability in the northern hemisphere. *J. Atmos. Sci.*, in press.

570 Thompson, D. W. J. and J. D. Woodworth, 2014: Barotropic and baroclinic annular vari-
571 ability in the southern hemisphere. *J. Atmos. Sci.*, **71**, 1480–1493.

572 Tian, B. and V. Ramanathan, 2003: A simple moist tropical atmosphere model: The role of
573 cloud radiative forcing. *J. Climate*, **16**, 2086–2092.

574 Vallis, G. K., 2006: *Atmospheric and Oceanic Fluid Dynamics: Fundamentals and Large-*
575 *Scale Circulation*. Cambridge University Press, Cambridge, U.K., 561 pp.

576 Wettstein, J. and J. Wallace, 2010: Observed patterns of month-to-month storm track vari-
577 ability and their relationship to the background flow. *J. Atmos. Sci.*, **67**, 1420–1437.

578 Zurovac-Jevtić, D., S. Bony, and K. Emanuel, 2006: On the role of clouds and moisture in
579 tropical waves: A two-dimensional model study. *J. Atmos. Sci.*, **63**, 2140–2154.

List of Figures

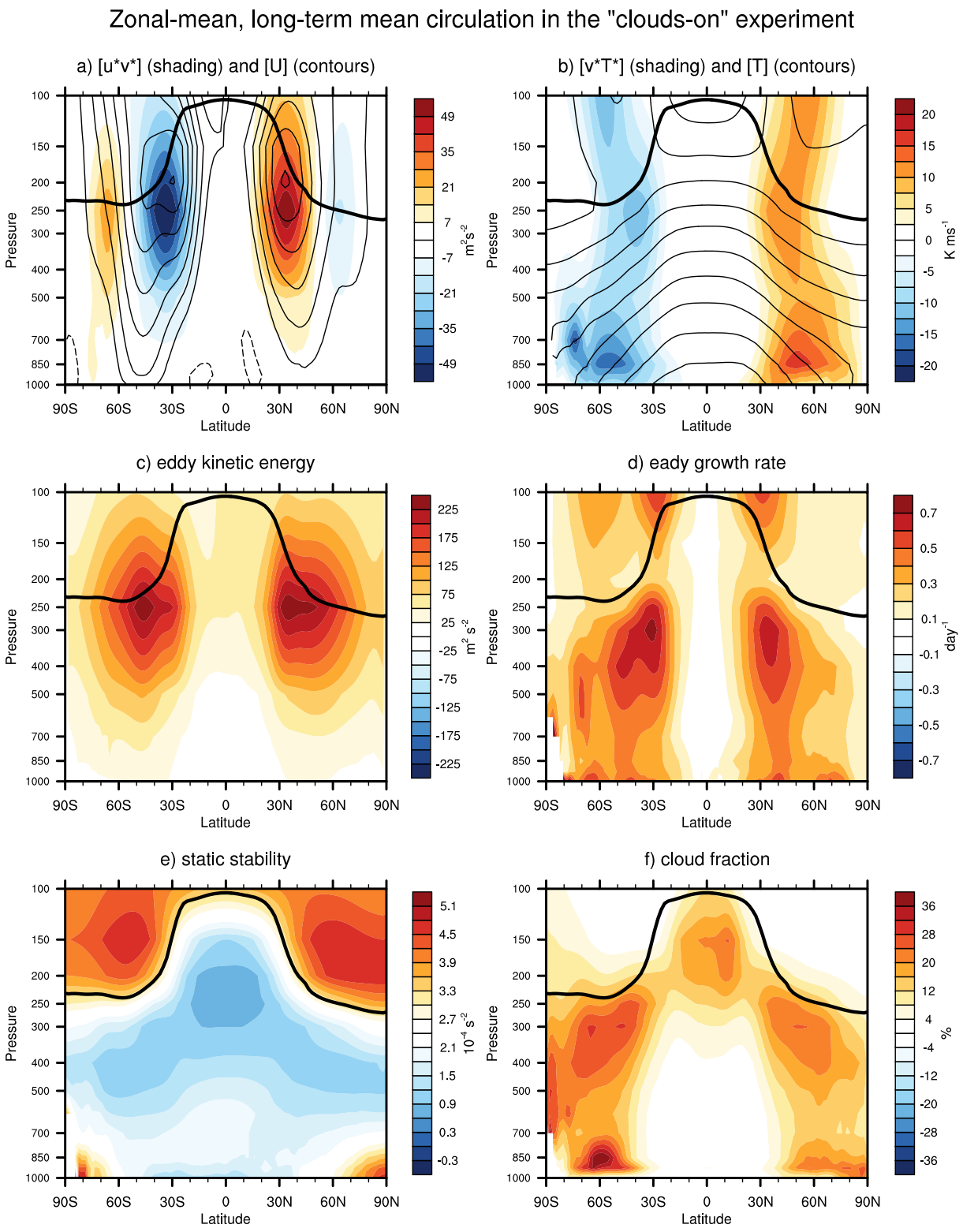

FIG. 1. The long-term mean, zonal mean circulation of the *clouds-on* experiment for the fields indicated. The contour intervals are 5 m s^{-1} in panel a, and 10 K in panel b. The thick solid line superimposed on each panel indicates the long-term mean tropopause height. In all results, long-term mean denotes the mean over all 30 years of the integration.

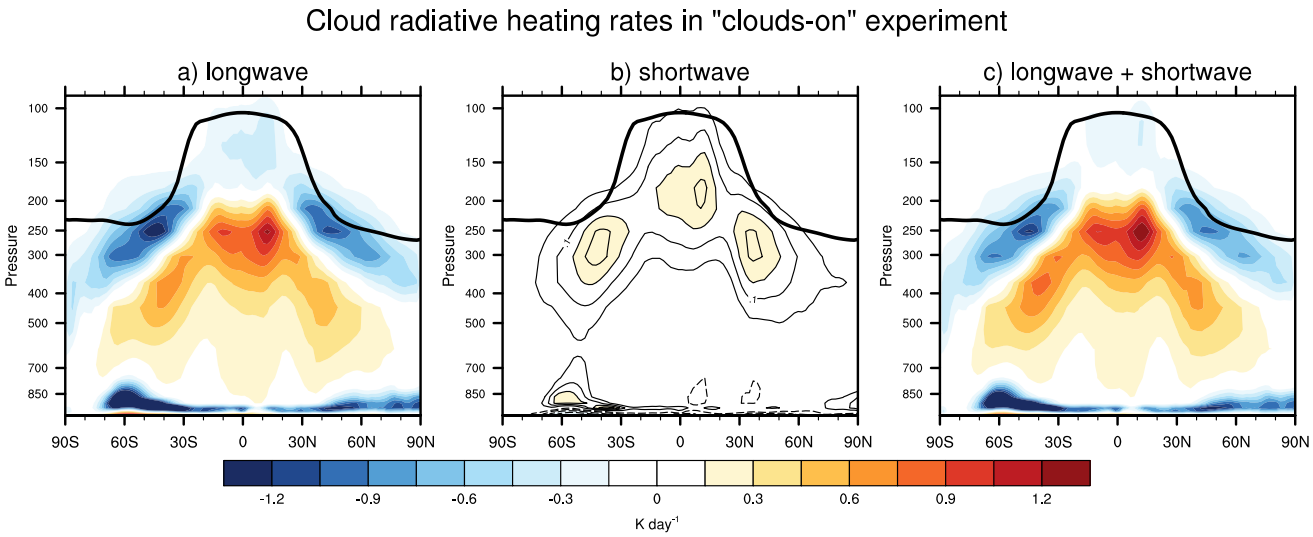

FIG. 2. The long-term mean, zonal mean cloud radiative effects in the *clouds-on* experiment: (a) the longwave component, (b) the shortwave component, and (c) the total cloud radiative effects. The contours in the middle panel are placed at 0.05 K day^{-1} and are included to help indicate the structure of the relatively weak shortwave forcing. The thick solid line superimposed on each panel indicates the long-term mean tropopause height in the "*clouds-on*" experiment.

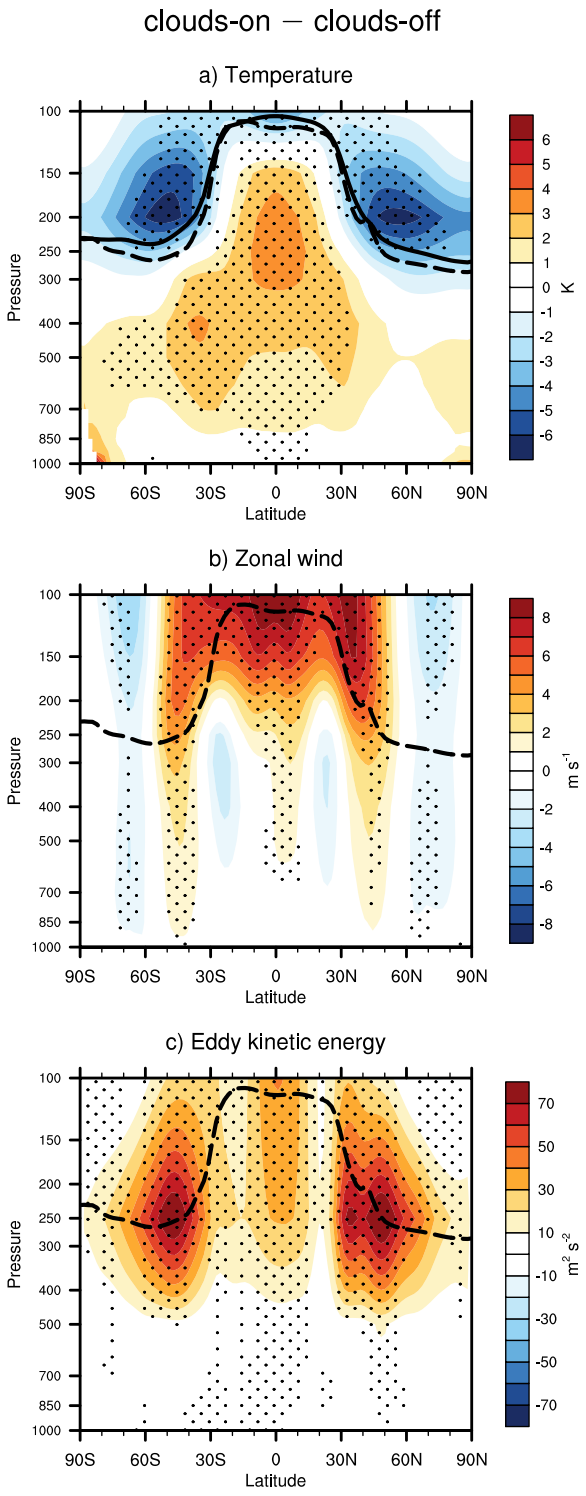

FIG. 3. Differences in the long-term mean, zonal-mean atmospheric circulation between the *clouds-on* and *clouds-off* experiments for fields indicated. Differences that are significant at the 99% level are stippled. The dashed lines in all panels indicate the long-term mean tropopause height in the *clouds-off* experiment. The solid line in panel (a) indicates the long-term mean tropopause height in the *clouds-on* experiment.

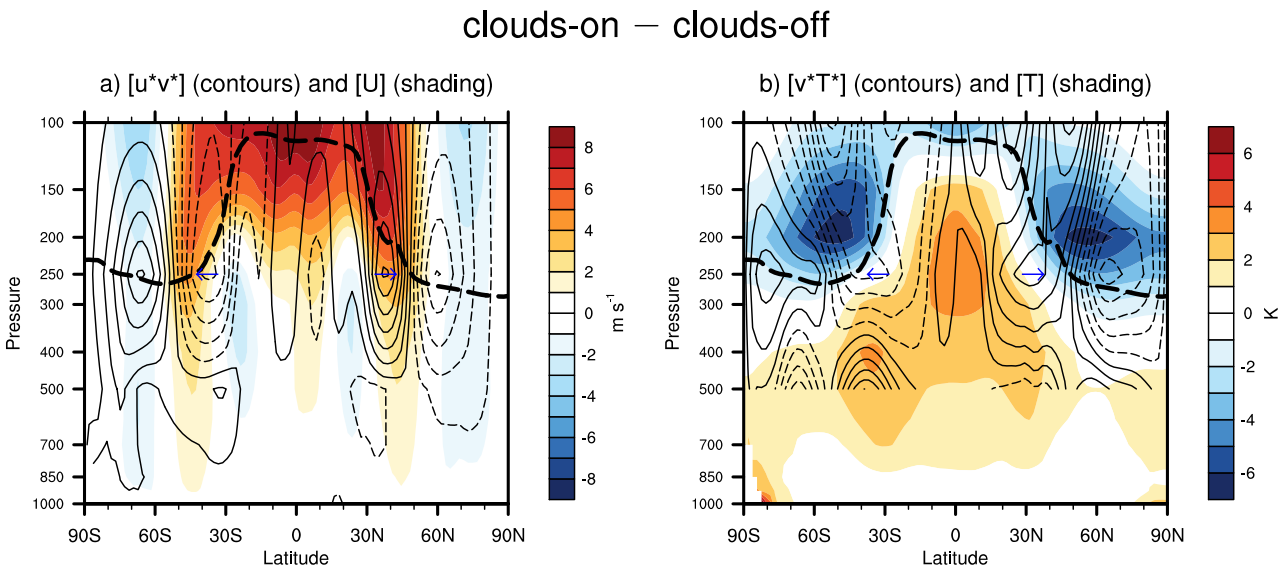

FIG. 4. Differences in the long-term mean, zonal-mean atmospheric circulation between the *clouds-on* and *clouds-off* experiments for fields indicated. The dashed lines in all panels indicate the long-term mean tropopause height in the *clouds-off* experiment. Eddy fluxes of heat below 500-hPa are masked out. Contours are shown at ...−3, −1, 1, 3... $m^2\ s^{-2}$ (left), and −0.6, −0.2, 0.2, 0.6... K m^{-2} (right). Note the zonal wind in (a) and temperature in (b) are reproduced from Figure 3. Horizontal arrows near 250 hPa at ∼40° indicate the direction of the eddy fluxes.

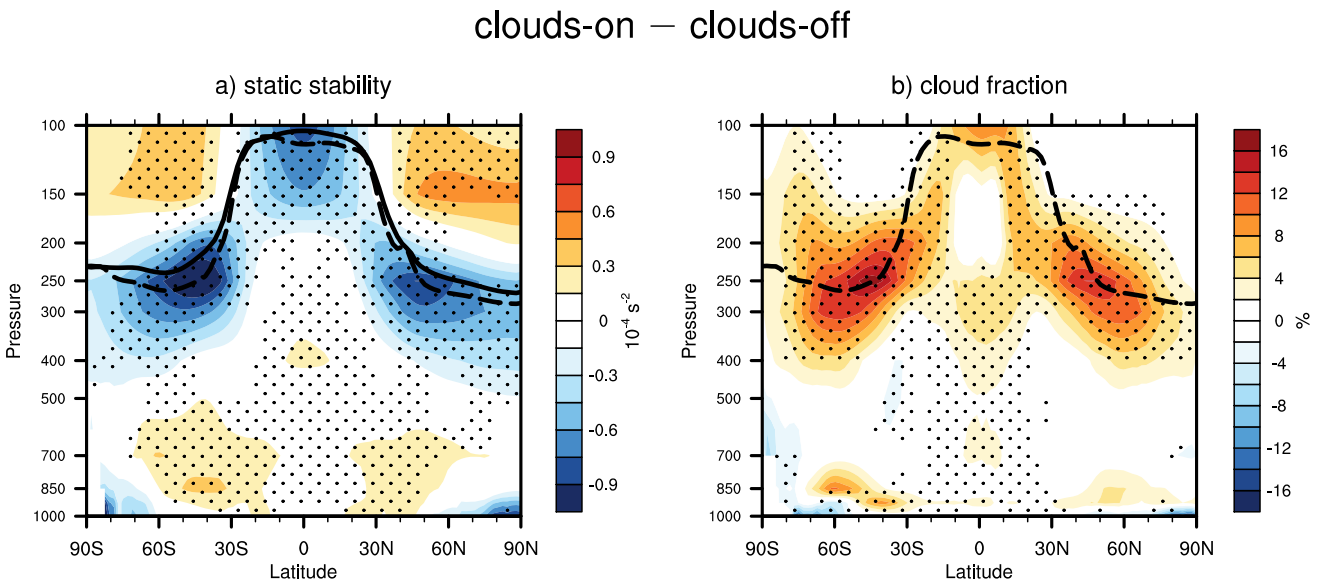

FIG. 5. Differences in the long-term mean, zonal-mean atmospheric circulation between the *clouds-on* and *clouds-off* experiments for fields indicated. Differences that are significant at the 99% level are stippled. The dashed lines in both panels indicate the long-term mean tropopause height in the *clouds-off* experiment. The solid line in panel (a) indicates the long-term mean tropopause height in the *clouds-on* experiment.

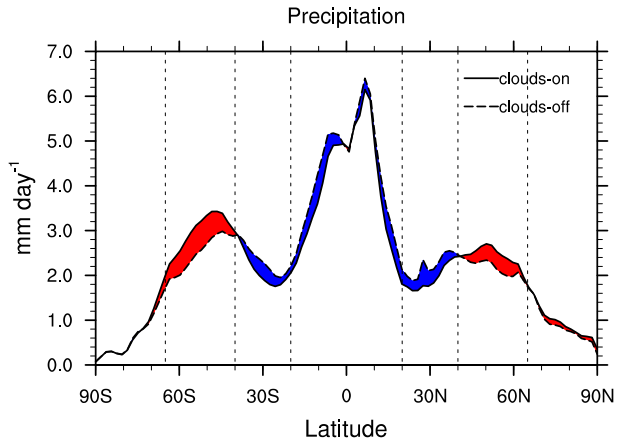

FIG. 6. The meridional structure of the long-term mean, zonal-mean precipitation in the *clouds-on* (solid line) and *clouds-off* (dashed line) experiments. Areas shaded in red indicate regions where precipitation in the *clouds-on* experiment exceeds that in the *clouds-off* experiment, and vice versa for areas shaded in blue. Vertical lines are drawn at 20°, 40°, and 60° latitudes for reference.

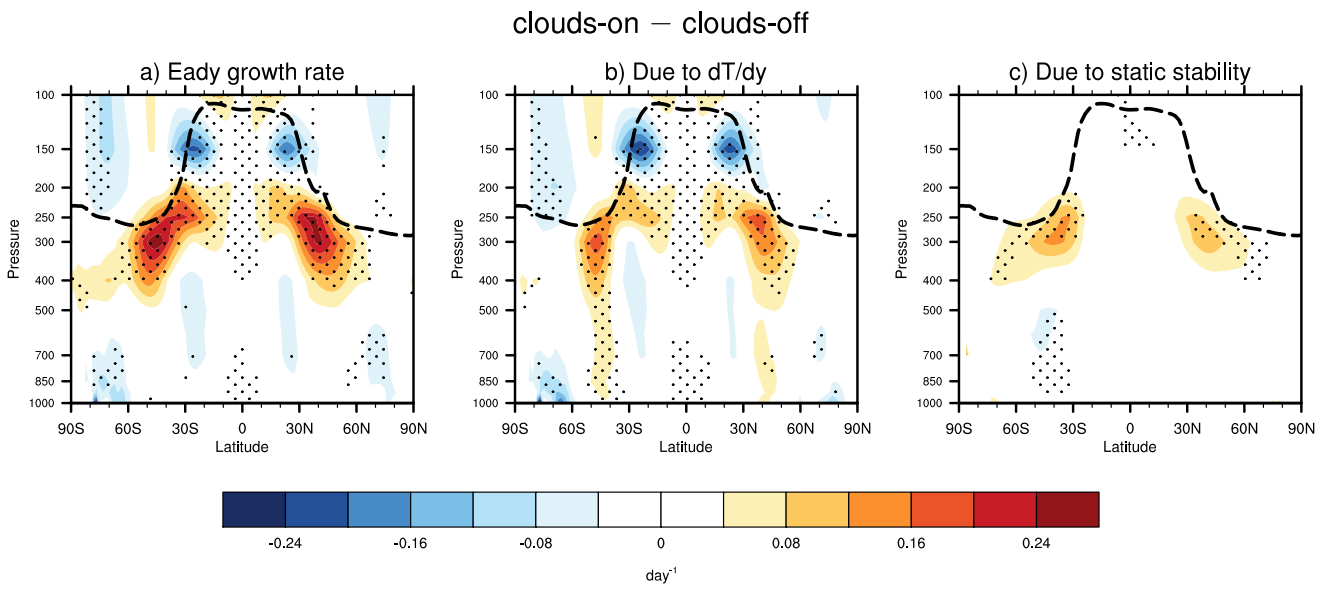

FIG. 7. Differences in the long-term mean, zonal-mean Eady growth rate between the *clouds-on* and *clouds-off* experiments. a) The differences in the total Eady growth rate; (b) the difference due to changes in the meridional temperature gradient and (c) the difference due to changes in the static stability. The dashed lines in all panels indicate the long-term mean tropopause height in the *clouds-off* experiment.

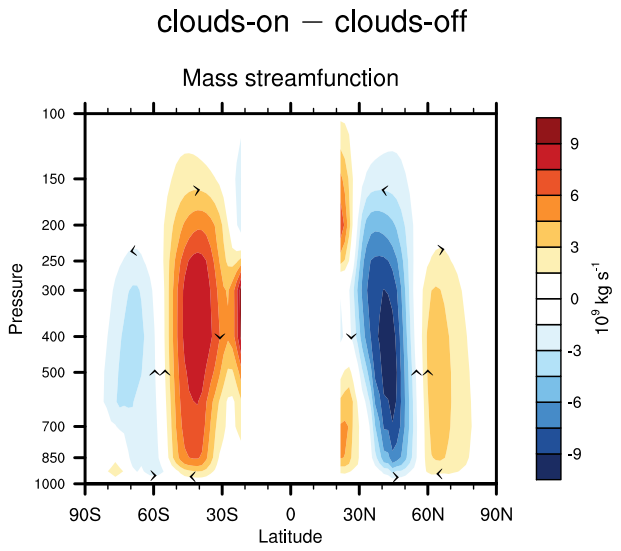

FIG. 8. Differences in the long-term mean, zonal-mean meridional overturning circulation between the *clouds-on* and *clouds-off* experiments. The meridional overturning circulation is shown as the zonal-mean mass streamfunction. Results are masked out in the tropics, where the results are spatially amporphous and not significant.

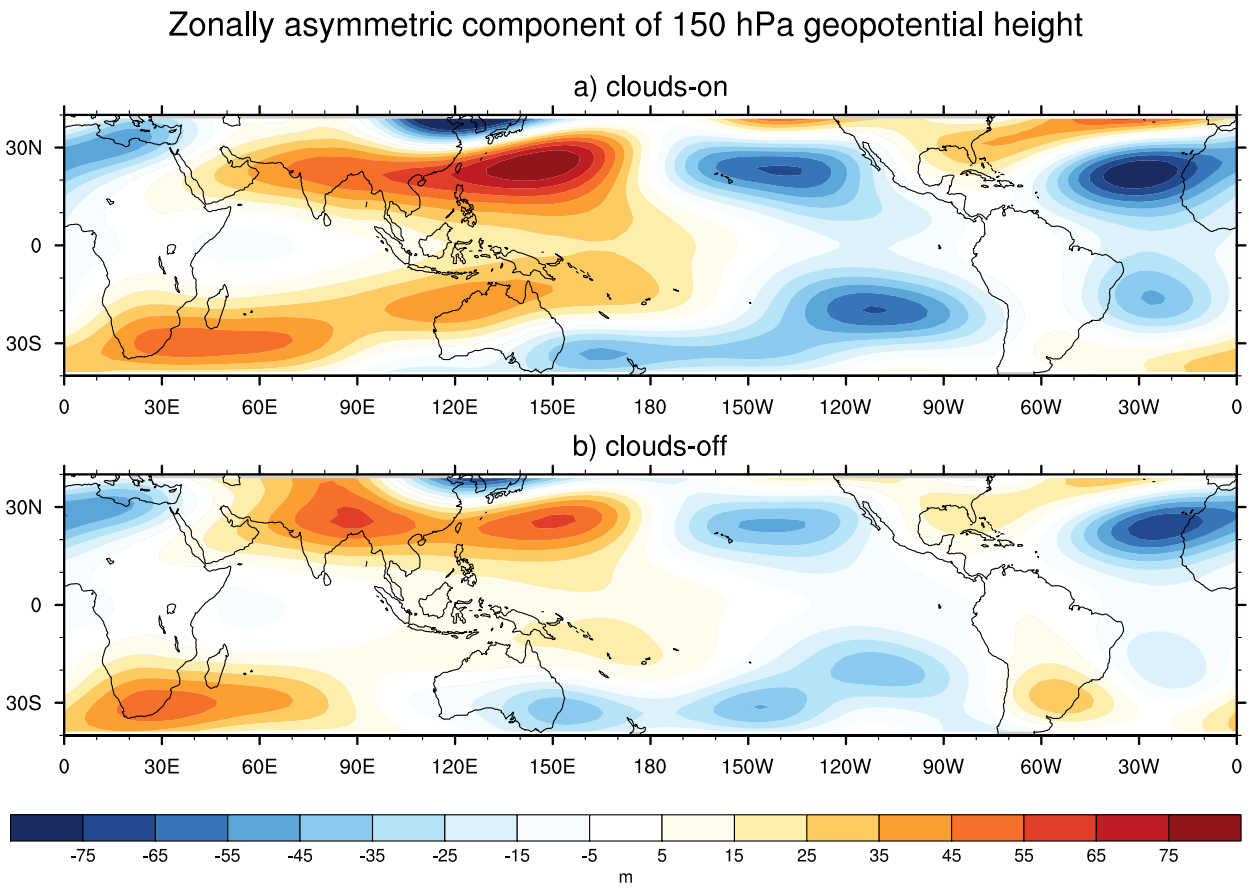

FIG. 9. Horizontal structure of the long-term mean, 150 hPa height field in the (a) *clouds-on* and (b) *clouds-off* experiments. Results show the zonal asymmetric component of the geopotential height at 150 hPa (i.e., the zonal-mean has been removed from the data).

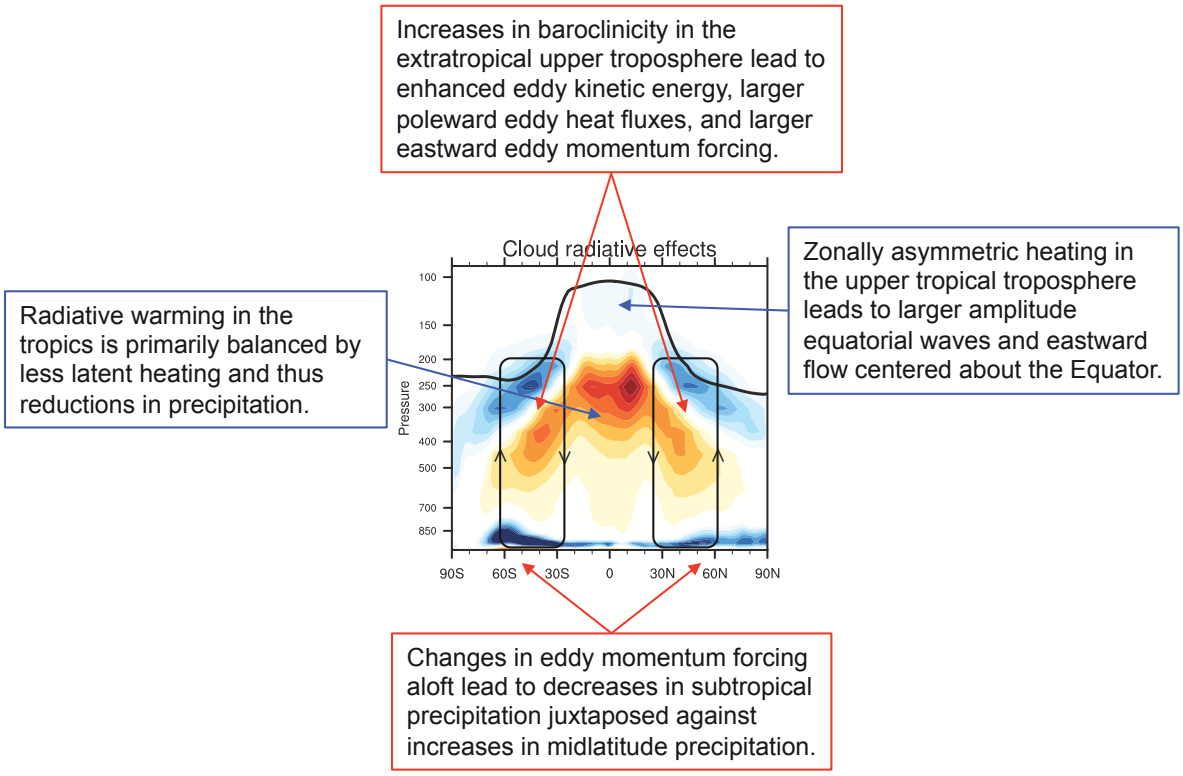

FIG. 10. Schematic diagram summarizing the basic impacts of cloud radiative effects on the zonal mean circulation, as revealed in this study. The shading is reproduced from Figure 2c and indicates the cloud radiative effects in the *clouds-on* experiment; the solid line indicates the long-term mean tropopause height from the *clouds-on* experiment.